Acta Crystallographica Section D
Biological Crystallography
ISSN 0907-4449

Structure of C73G putidaredoxin from *Pseudomonas putida*

Natasha Smith,[a] Martin Mayhew,[a]‡ Marcia J. Holden,[a] Halonna Kelly,[a] Howard Robinson,[b] Annie Heroux,[b] Vincent L. Vilker[a] and D. T. Gallagher[a]*

[a]Biotechnology Division of the National Institute of Standards and Technology, Gaithersburg, MD 20899-8312, USA, and [b]Biology Department, Brookhaven National Laboratory, Upton, NY 11973, USA

‡ Current address: Biocatalytics Inc., Pasadena, CA 91105, USA.

Correspondence e-mail: travis.gallagher@nist.gov

Received 2 December 2003
Accepted 11 February 2004

PDB Reference: C73G putidaredoxin, 1r7s, r1r7ssf.

The structure of the C73G mutant of putidaredoxin (Pdx), the Fe_2S_2 ferredoxin that supplies electrons to cytochrome CYP101 (P450cam) for camphor oxidation, is reported at 1.9 Å resolution in a *C*2 crystal form. The structure was solved by single-wavelength iron anomalous diffraction, which yielded electron density above the 2σ level for over 97% of the non-H atoms in the protein. The final structure with $R = 0.19$ and $R_{\rm free} = 0.21$ has been deposited in the Protein Data Bank with accession code 1r7s. The *C*2 crystal contains three Pdx molecules in the asymmetric unit, giving three independent models of the protein that are very similar (r.m.s.d. < 0.3 Å for the 106 C^{α} atoms). The unusually high solvent fraction of 80% results in comparatively few crystal-packing artifacts. The structure is briefly compared with the recently reported crystal structures of the C73S and C73S/C85S mutants. In general, the eight independent molecules in the three crystal structures (three in C73G, three in C73S and two in C73S/C85S) are much more similar to each other than to the previously reported NMR structure of wild-type Pdx in solution. The present findings show a unanimous structure in some regions crucial for electron-transfer interactions, including the cluster-binding loop 39–48 and the cytochrome-interaction region of Asp38 and Trp106. In addition, the Cys45 amide group donates a hydrogen bond to cluster sulfur S1, with Ala46 adopting an Lα conformation, in all three molecules in the crystal.

1. Introduction

Fe_2S_2 ferredoxin proteins utilize bound iron–sulfur clusters to carry electrons in a wide variety of functions and organisms. The structures of about 20 such proteins with chain lengths of 94–128 amino acids have been determined by crystallographic or NMR methods and have been deposited in the PDB (Berman *et al.*, 2002). The majority have a common fold similar to that of ubiquitin (Vijay-Kumar *et al.*, 1987), but containing four conserved cysteines that coordinate the irons of the redox-active cluster. (The exception is the thioredoxin-like fold represented by the Fe_2S_2 ferredoxin from *Aquifex*; PDB code 1m2a; Yeh *et al.*, 2000.) In the predominant fold, three of the four iron-binding cysteines are contributed by a surface loop near the middle of the sequence, positioning the cluster near the surface for efficient electron transfer.

Putidaredoxin is a 106-residue (11.6 kDa) ferredoxin that is produced in *Pseudomonas putida*. It carries electrons from the flavoprotein putidaredoxin reductase (PdR) to the acceptor cytochrome CYP101, also known as P450cam because it catalyzes camphor hydroxylation. This NADH-supplied electron-transfer chain is one of the best studied of the P450 systems, which have been reviewed by Mueller *et al.* (1995). The structure of Pdx was determined by NMR methods

Table 1
Crystal, diffraction and refinement statistics.

Values in parentheses are for the outer resolution shell.

Crystal statistics	
Dimensions (μm)	100 × 50 × 40
Space group	C2
Unit-cell parameters (Å, °)	a = 145.08, b = 78.22, c = 55.74, α = 90.0, β = 111.33, γ = 90.0
Molecules per AU	3
V_M (Å^3 Da^{-1})	4.2
Solvent content (%)	80
Diffraction statistics	
Wavelength (Å)	1.6
Temperature (K)	100
Resolution shell (Å)	30–1.91 (1.98–1.91)
Observations	313135 (20755)
Unique reflections	45116 (4482)
Completeness (%)	100.0 (99.9)
Redundancy	6.9 (4.6)
Mean $I/\sigma(I)$	15.6 (6.1)
Reflections with $I > 3\sigma$ (%)	89.4 (66.4)
R_{merge}† (%)	0.083 (0.266)
Refinement	
Resolution range (Å)	10–1.91
No. reflections in working set	40889
No. reflections in test set	2131
No. protein atoms	2388
No. solvent molecules	303
No. ligand atoms	12
R overall‡ (%)	18.9
R_{free}‡ (%)	21.4
R.m.s. deviation, bond lengths (Å)	0.020
R.m.s. deviation, bond angles (°)	2.02
Estimated coordinate error σ_A (Å)	0.11

† $R_{merge} = \sum |I_i - \langle I \rangle| / \sum I_i$, where I_i is the intensity of the ith observation and $\langle I \rangle$ is the mean of the observed intensities for each reflection. ‡ $R = \sum |F_o - F_c| / \sum F_o$.

(Pochapsky *et al.*, 1994) and subsequently refined (Pochapsky *et al.*, 1994; PDB code 1pdx). Owing to the magnetic properties of iron, NMR resonances for atoms within ∼8 Å of the cluster are distorted and thus NMR methods are of limited effectiveness in the protein region of greatest interest. The electronic properties and redox interactions of Pdx have been extensively studied (Davies & Sligar, 1992; Lyons *et al.*, 1996; Unno *et al.*, 1996; Holden *et al.*, 1997; Roitberg *et al.*, 1998; Sari *et al.*, 1999). These studies and others cited therein have utilized various methods including Raman, NMR, modeling, mutagenesis and activity measurements. Pdx carries one electron at a time, such that the two irons switch between [Fe^{3+}, Fe^{3+}] (oxidized) and [Fe^{2+}, Fe^{3+}] (reduced) states. Mutational and other evidence indicates that helix *G* (residues 64–72) is important for interaction with the reductase and that Asp38 and the C-terminal Trp106 are important for binding the cytochrome. Outstanding questions center on the differential structural features of the two redox states of Pdx and on the modes of binding and mechanisms of electron transfer with PdR and CYP101.

The need for better structural information on Pdx has motivated extensive crystallization efforts. Crystal structures of the C73S and double C73S/C85S mutants of Pdx have recently been reported (PDB codes 1oqq and 1oqr; Sevrioukova *et al.*, 2003), providing five independent images of the molecule (owing to non-crystallographic symmetry in the tetragonal and orthorhombic forms) that are generally consistent and are significantly different from the NMR model. Here, we report the crystal structure of the C73G mutant. This surface mutation facilitates crystallization without affecting cluster ligation and with only minor effects on activity: its activities were previously reported as 60% of the wild type for reduction and 95% for oxidation (Holden *et al.*, 1997). The native iron enabled highly effective phasing, so that the resulting maps are easily interpreted to resolve without assumptions many detailed questions regarding the structure of this protein.

2. Materials and methods

Pdx was expressed and purified as described by Grayson *et al.* (1996) and concentrated to 40 mg ml^{-1} (3.4 m*M*) in 20 m*M* K_2HPO_4 pH 7.4, with 20 m*M* KCl, 5 m*M* dithiothreitol and 0.01% NaN_3 for crystallization. The protein absorbs light in the visible range and its solutions are a dark red color. The following mutants were prepared similarly and also screened for crystallization: H8Y, E72Q, C73G, C73R, E77Q, D95H and W106Δ (deletion of the C-terminal tryptophan residue). Initial screening was by vapor diffusion with Crystal Screens 1 and 2 from Hampton Research using hanging drops at room temperature (∼297 K) and sitting drops at 277 K. It was observed that conditions with pH values of 6 or below invariably produced precipitate and bleaching (loss of color), indicating that the Fe_2S_2 cluster had been released from the protein. Slow-growing needle-like crystals of the C73G mutant were produced using condition 16 of Screen 1 (1.5 *M* Li_2SO_4, 0.1 *M* HEPES pH 7.5) at 277 K. Although these crystals were small and thin (dimensions of 10 × 10 × 100 μm), they were clearly reddish in color. The crystals were eventually reproduced and the salt concentration was optimized to 1.8 *M*. The habit remained needle-like until Detergent Screen 1 was applied; more isometric crystals were obtained when 2 m*M* *n*-octanoyl sucrose was added. The crystals were now better shaped, but usually highly compound, appearing as florid clusters, and required months for growth. In rare cases a cluster would develop to the point where a single crystallite of size ∼100 × 100 × 100 μm could be broken off and mounted for diffraction.

A Pdx crystal was utilized for diffraction and single-wavelength anomalous dispersion (SAD) phasing at Brookhaven National Laboratory beamline X26c. The wavelength 1.6 Å was chosen to ensure a strong Fe anomalous signal (the *K* edge is at 1.74 Å). Diffraction data to 1.9 Å resolution were collected (see Table 1) at 100 K, reduced using *SCALEPACK* (Otwinowski & Minor, 1997) and phased using the program *SOLVE* (Terwilliger & Berendsen, 1999). The program's automatic Patterson interpretation located the six iron sites and calculated the phases for the map shown in Figs. 1, 2 and 5. The map is of sufficient quality that over 97% of the main-chain carbonyl groups are observed at the 3σ contour level. *SOLVE*'s automatic chain-tracing feature (*RESOLVE*) correctly traced 94% of the 318 residues in the asymmetric unit. Manual model building using the program *Xfit* (McRee,

1999), still fitting to the measurement-phased map, enabled completion of the model, except for the distal side-chain atoms of 14 residues, mostly Lys and Glu. This model, before any refinement, had an R value of 0.29 over the resolution range 10–4 Å.

The structure was found to contain only three molecules in the asymmetric unit, giving it the unusually high solvent fraction of 80% (V_M = 4.2 Å^3 Da^{-1}). In the refinement using the program *CNS* (Brünger *et al.*, 1998), restraints were removed for Cys-to-Fe coordination geometry (lengths, angles and dihedrals) and for Fe_2S_2 cluster planarity. Simulated annealing reduced R to 0.26 for the resolution range 10–2.2 Å. R_{free}, calculated over a random subset containing one-twentieth of the reflections, was 0.27 for the same resolution range. Refinement continued with alternating passes of energy minimization, map inspection and manual adjustments, resulting in R = 0.19 and R_{free} = 0.21 for data to 1.91 Å. Statistics for the refined model are included in Table 1. The final model including 303 water molecules was deposited in the Protein Data Bank with accession code 1r7s.

3. Results

The experimentally phased SAD (single-wavelength anomalous dispersion) electron-density map, with no model or interpretation bias, reveals a complete unambiguous chain trace at the 2σ contour level and includes 95% of the backbone carbonyls at the 3σ level. Fig. 1(*a*) shows the map (and the refined structure) in the region of the Fe_2S_2 cluster of Pdx molecule *A*. Fig. 1(*b*) likewise shows the map in the region of the C-terminus of molecule *B*. 100% of the residues (all three molecules) are within either the 'core' or the 'additional allowed' regions of Ramachandran space (Laskowski *et al.*, 1993). The mean B values for the three protein molecules are 20.4, 20.2 and 22.4 Å^2, in reasonable agreement with the Wilson B value of 20.1 Å^2. The B values for all the Fe_2S_2 atoms are in the range 16–24 Å^2. There are 160 atoms (7% of the protein) with B values over 30 Å^2; these atoms are generally the distal atoms of surface side chains, which are normally somewhat mobile. Electron density is weak (below 1.5σ) for most of these atoms and it may be a useful practical guideline to consider atoms with B > 30 Å^2 to be poorly ordered.

The three independent models of Pdx in the asymmetric unit are very similar, with pairwise r.m.s.d. values of between 0.20 and 0.26 Å for C^α atoms and of between 0.65 and 1.09 Å for all non-H atoms. Fig. 2 shows a superposition of the three independent models of Pdx. In general, the structures align closely and all the main-chain atoms superimpose within 0.6 Å (so that the Ramachandran plots are virtually identical). There are about ten side chains that do not align, adopting different rotamers in one or more of the three structures; most of these side chains are on the surface and are clearly perturbed by contact with a neighboring Pdx molecule in the crystal.

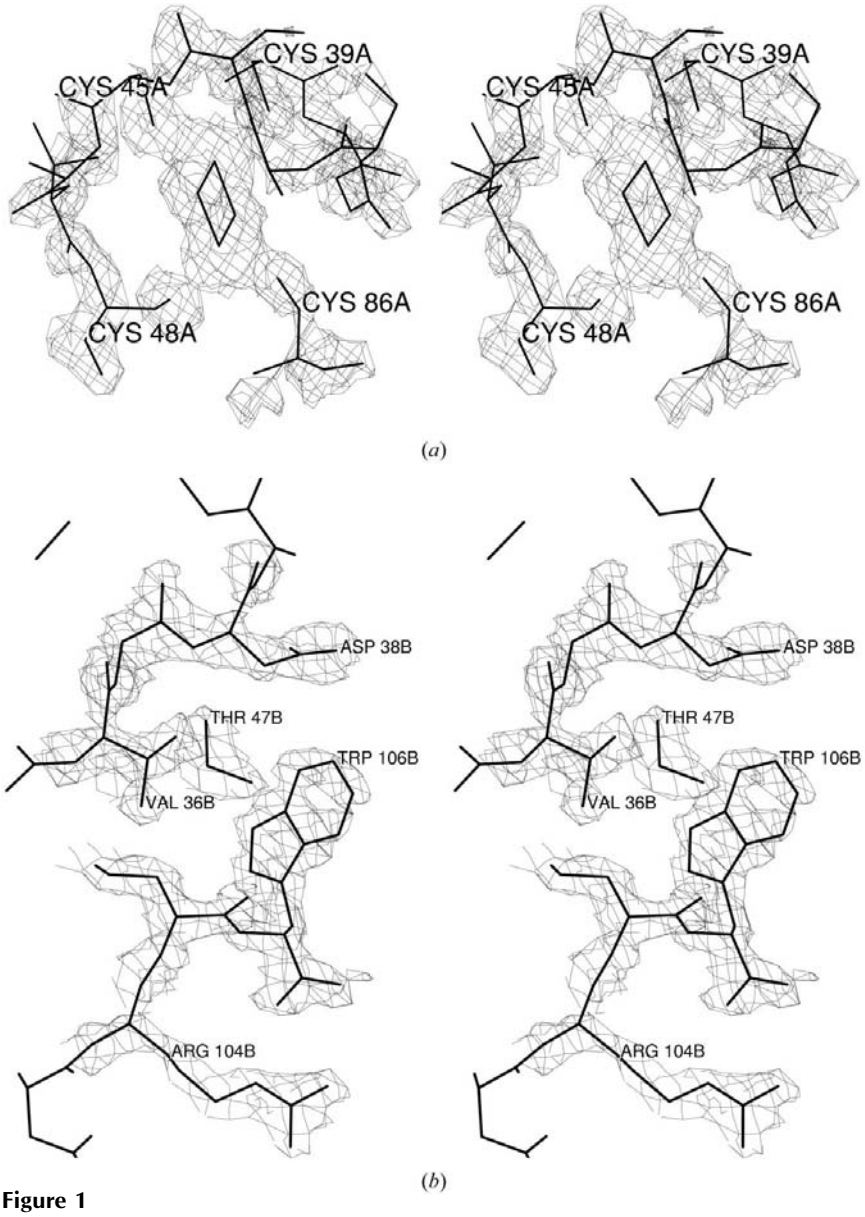

Figure 1
Stereo diagrams of the unbiased SAD (single-wavelength anomalous dispersion) map. (*a*) The region of the Fe_2S_2 cluster of the *A* chain contoured at the 3σ level. The refined model is superimposed. Although a few side-chain atoms are not included in the electron density at this level, all the main-chain atoms and carbonyls are and the map interpretation is unambiguous with regard to main-chain conformation and side-chain rotamers. (*b*) The region of Asp38 and the C-terminal Trp106 of the *B* chain contoured at the 2σ level, showing that these two side chains are in van der Waals contact (separation 3.5 Å). Also evident is the hydrogen-bond interaction between the C-terminal carboxylate and the side chain of Arg104. Molecules *A* and *C* are similarly structured in this region. The figure was produced using *XtalView* (McRee, 1999).

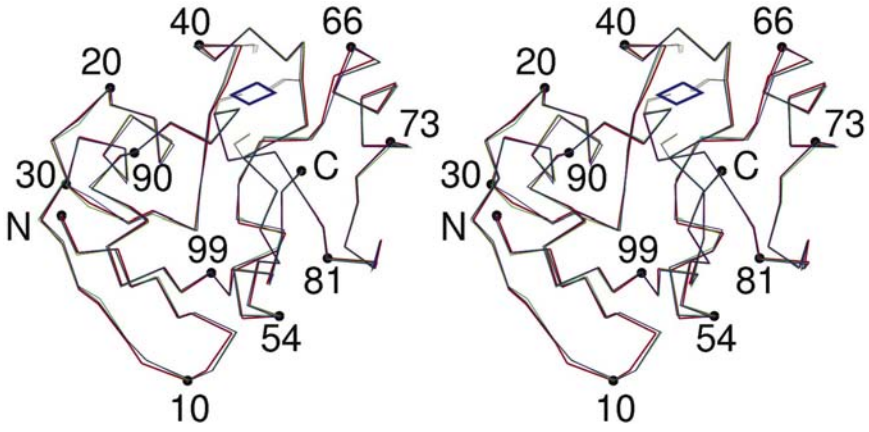

Figure 2
Stereo superposition (C^{α} trace) of the three independent Pdx molecules in the asymmetric unit, showing the sequence numbering and the close similarity (pairwise r.m.s. deviations 0.20–0.26) of the three structures. The side chains of the four iron-binding cysteines are added; the Fe_2S_2 cluster is the rhombus near the top of the figure.

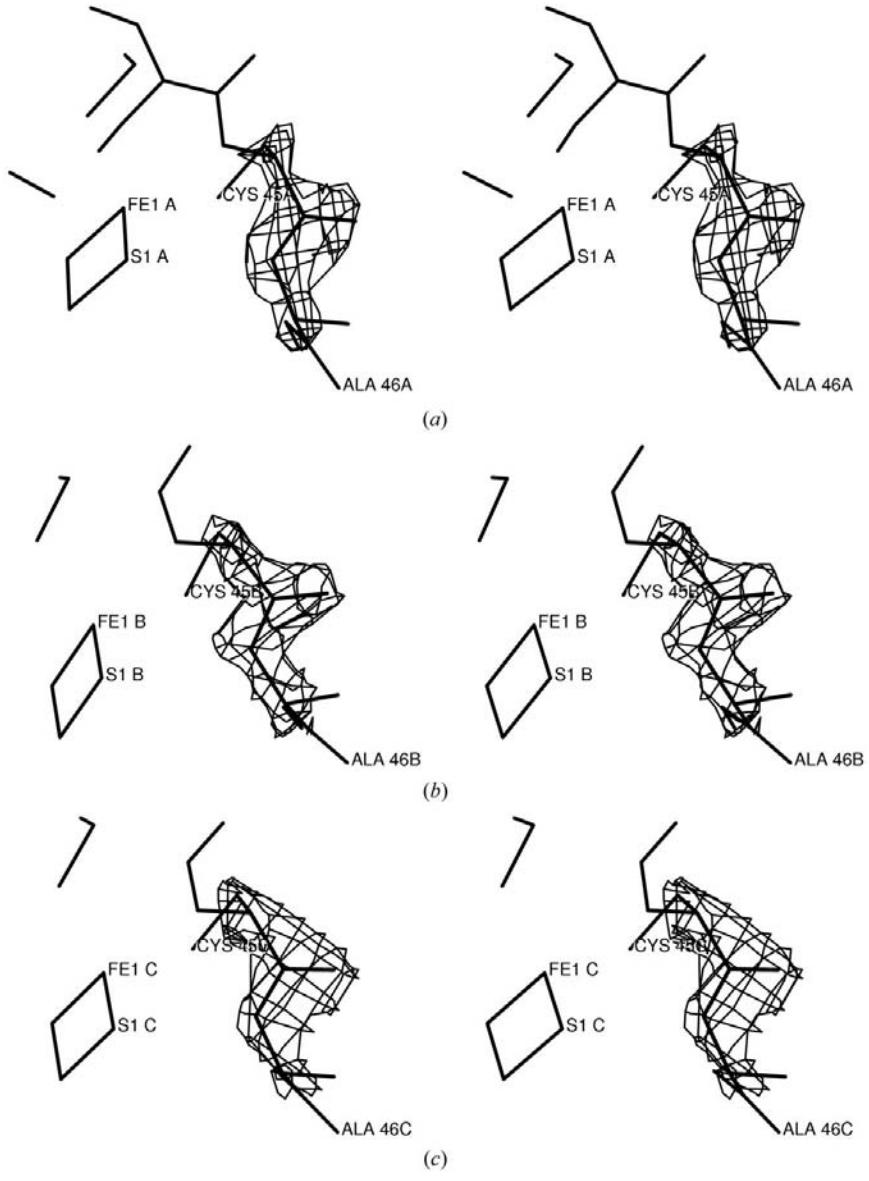

The three independent observations of the Pdx structure agree closely in the region surrounding the Fe_2S_2 cluster. Defining this region by the residue zones 24, 35–49 and 84–87 gives an approximate 8 Å radius around the cluster. Within this region, the three molecules have no discrepant rotamers and all atoms superimpose to within 0.5 Å. Interestingly, all five cysteines (including the four that coordinate iron) have χ_1 values near +70°, which is the least favorable, most sterically restrictive rotamer and is rare for Cys. Also in this region two non-glycine residues, Ala43 and Ala46, are observed to have a left-handed α (Lα) conformation in all three models. Fig. 3 shows the unbiased electron-density map at the 45–46 peptide bond in each of the three independent molecules (see §3).

In the initial map, the peaks for the four atoms in each cluster appeared to be coplanar. Nevertheless, the cluster coordination geometry was refined without restraints in order to obtain a model unbiased by geometric restraints. Specifically, all restraints on Cys—Fe bonds were removed (lengths, angles and torsions) as well as the planarity of the cluster itself. Based both on the locations of the four peaks for each cluster in the experimental map and on the unrestrained final model, the cluster appears to be planar within the coordinate error of about 0.11 Å.

The protein grips the Fe_2S_2 cluster chiefly by the surface loop formed by residues 37–48 (Figs. 1, 2, 4 and 5). This loop provides three of the four cysteines that ligate the Fe atoms (cysteines 39, 45 and 48); Cys86 is the fourth Fe binder. The residues surrounding the cluster show a distinct pattern, with their carbonyl groups directed outward and their amide groups inward. As a result, three main-chain amides donate hydrogen bonds to the cluster sulfurs and six main-chain amides donate hydrogen bonds to the four cysteine sulfurs that coordinate the Fe

Figure 3
Stereo diagrams of the unbiased SAD map (3σ contour level) showing the Lα (left-handed α) conformation of Ala46 in each of the three Pdx molecules. The final model is superimposed. As a result of this conformation, the peptide carbonyl points outward, away from the cluster, and the amide donates a hydrogen bond to the cluster S1 atom (see Fig. 4) in all three independent molecules in the crystal. The figure was produced using *XtalView* (McRee, 1999).

Table 2
Hydrogen bonds to cluster sulfurs and to cluster-ligating sulfurs, using a 3.6 Å distance cutoff and, for N—S interactions, a 40° angle cutoff (measured as the deviation of the NS vector from the peptide plane).

		Distance in molecule			
Acceptor	Donor	*A*	*B*	*C*	Acceptor Fe ligand
S1	45N	3.55	3.58	3.43	
	46N	3.41	3.48	3.33	
S2†	41N†	3.41	3.34	3.37	
39S	41N	3.50	3.60	3.52	Fe1
	42N	3.43	3.32	3.32	
	42O$^{\gamma}$	3.69‡	3.55	3.49	
	44N	3.36	3.37	3.37	
45S	39N	3.37	3.33	3.37	Fe1
	47N	3.32	3.42	3.46	
	47O$^{\gamma}$	3.08	2.90	3.13	
48S	86N	3.54	3.48	3.48	Fe2
86S	87N^{e}	3.30	3.33	3.32	Fe2

† This interaction is weak because the angle is >30°. ‡ This distance, although >3.6 Å, is included because in molecules *B* and *C* it is <3.6 Å.

atoms. In addition to these main-chain donors, three side chains (Ser42, Thr47 and Gln87) have donors within hydrogen-bonding distance of an iron-binding cysteine sulfur. In total, there are seven hydrogen bonds donated to the Cys ligands to Fe1 and two donated to the Cys ligands to Fe2 (Table 2).

4. Discussion

Structurally characterized members of the Pdx-fold family now include representatives from all three major branches of the tree of life. Plants and cyanobacteria so far provide the most examples; in these cases, the proteins carry photosynthesis-derived electrons to various acceptors. The greatest structural difference between Pdx and most of these homologs is in the region of helix *G* (residues 64–72). This region is shorter in the archaeal, plant and cyanobacterial homologs and the C-terminus extends to fill the gap. Two proteins from *Escherichia coli* (ferredoxin, PDB code 1i7h and terpredoxin, PDB code 1br9) and the bovine mitochondrial homolog adrenodoxin (PDB code 1ayf) have the same arrangement of these elements as Pdx, in which the C-terminus approaches the Fe_2S_2 cluster (Kostic *et al.*, 2002). In addition to this similarity, the adrenodoxin structure (Muller *et al.*, 2001) is in complex with its cognate reductase, thus providing a valuable homologous model for the Pdx–PdR interaction.

The structures of the three molecules of C73G Pdx are generally similar to the five independent mutant structures reported by Sevrioukova *et al.* (2003): the pairwise r.m.s. deviations in the C$^{\alpha}$ positions range from 0.27 to 0.51 Å. The backbone conformations superimpose closely except for the 45–46 peptide (see below). There are some dozen well ordered side chains with different rotamers including Val3, Asp9, Val60 and Met90, but none of these are within 10 Å of the cluster. The present findings agree with Sevrioukova *et al.* (2003) regarding the conformation of the protein in the 33–38 region, including the observation of Tyr33 on the protein surface. Moreover, the observed adjacent conformations of Asp38 and Trp106 (Fig. 1*b*) are in agreement with the predominant conformations reported for the C73S and C73S/C85S mutants, as is the internal packing around His49, which serves to link the active-site and interaction regions. The general differences between crystal and NMR structures, as reported by Sevrioukova *et al.* (2003), are maintained in the present structure, where the pairwise r.m.s. deviations (from model 1 of 1pdx) in the C$^{\alpha}$ positions range from 1.9 to 2.0 Å (Fig. 5).

Owing to the high solvent content of the C73G crystals, the protein surfaces are less perturbed by crystal contacts and the C73G structures are more internally consistent both in global terms (r.m.s.d., rotamer distributions) and in terms of particular functional regions. Unbiased electron density shows that the three C73G structures are in close agreement in several areas where the C73S and C73S/C85S structures contain packing-induced disparities. One such area is the C-terminus, where the hydrogen bond to the guanidine group of Arg104 is observed in all three C73G structures. Another region where the paucity of crystal contacts seems to give the present structures greater uniformity is the cluster-binding loop, where in the three molecules the rotamers of the hydrogen-bond-linked Ser42 and Ser44 are identical, and the side chain of Arg66 forms similar interactions with these serines, partly shielding the cluster from solvent (Fig. 5).

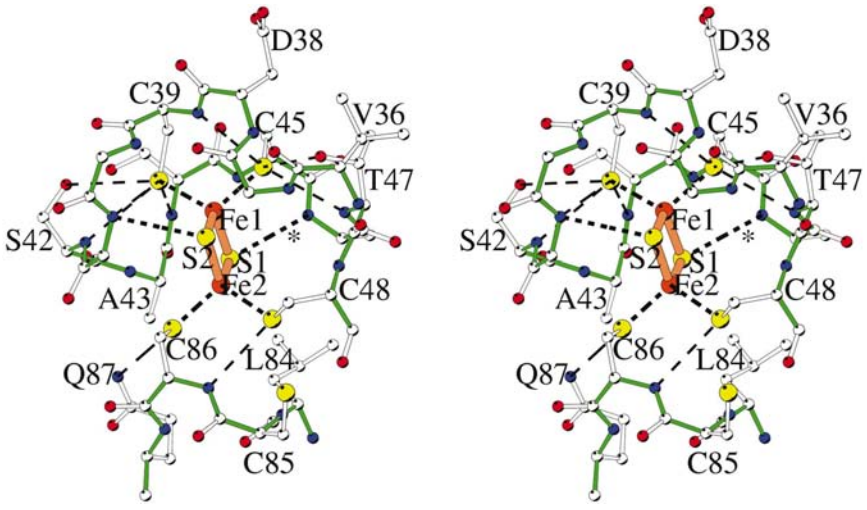

Figure 4
Diagram of the crystal structure (molecule *A*) in the Fe region. C atoms are colored white; other atoms have their usual colors. Bonds are colored green for backbone and white for side chains. Dotted lines show the four Cys—Fe bonds and two of the three hydrogen bonds from main-chain amides to the cluster sulfurs (41N–S2, distance 3.41 Å; 46N–S1, distance 3.41 Å); omitted for clarity is the 3.55 Å interaction 45N–S1. Dashed lines show the nine hydrogen bonds to the four cysteine sulfurs (Table 2). Omitted for clarity are the two Met residues at either end of the cluster: Met70 close to S1 and Met24 adjacent to S2. Note the general tendency for carbonyls to point away from the cluster. Figure produced using *MOLSCRIPT* (Kraulis, 1991).

In the region of the Fe_2S_2 cluster, there are two residues, Ala43 and Ala46, that clearly adopt a left-handed α conformation in all three molecules in the asymmetric unit. These are the only two Lα residues in the protein. While Ala43 is consistently Lα in all reported structures, Ala46 is in the more common right-handed α conformation in the NMR structure. Fig. 3 shows the unbiased electron-density map in the three instances of the 45–46 peptide bond. Interestingly, this bond has been conjectured to switch between the two conformations during the redox cycle in the *Anabaena* homolog, where a partially reduced crystal structure was reported (Morales *et al.*, 1999). In that study, it was suggested that in the oxidized structure the peptide flips to point its carbonyl inward, toward the more positively charged cluster, while in the reduced structure the carbonyl points outward. In the C73S (PDB code 1oqr) crystal structure, the conformation is Lα, while in the C73S/C85S (PDB code 1oqq) structure it is Rα. Although non-glycine residues adopt the Lα conformation with a frequency of only ∼0.005 (Richardson & Richardson, 1989), in context Lα appears more energetically favorable for Ala46 as the Rα conformation places the carbonyl O atom within 3 Å of both the cluster S1 and the Met70 side chain and results in residue Cys45 having unfavorable Ramachandran angles. In the present case with C73G Pdx, where the molecules are presumably in the oxidized state (although 5 m*M* DTT was present with the purified protein, no reducing agent was used in the crystal conditions and crystals required months to grow), the conformation is clearly Lα in all three cases, with the carbonyl pointing outward. Because the 45–46 peptide contacts sulfur S1 and because Cys45 is an Fe1 ligand, the conformation of this peptide is likely to affect the redox potential of the cluster (Figs. 4 and 5).

The solvent fraction of 80% is an unusual feature of these Pdx crystals. As a result of this low packing density, most of the protein surfaces are exposed to solvent and only a few surface residues are involved in contacts in all three of the independent molecules. Surprisingly, the surface-exposed C73G mutation site is not involved in crystal contacts in any of the three molecules, leaving it unclear how the mutation facilitated crystallization (we were unsuccessful at growing crystals of wild-type protein, even by seeding; besides C73G, the only other mutant that produced crystals in our study was C73R). It appears that the presence of the exposed Cys73 may interfere with crystal growth without simply disrupting a necessary contact interaction. It is probable that the cysteine, which is the only exposed Cys in wild-type Pdx, prevents crystallization by unfavorable (dimer-promoting) self-interactions, as suggested by Sevrioukova *et al.* (2003).

Pdx surface regions involved in its binding (and electron-transfer) interactions with cytochrome CYP101 and PdR have been analyzed in several previous studies. Helix *G* (residues 64–72) has been implicated in binding PdR (Holden *et al.*, 1997; Muller *et al.*, 2001) and the region of the C-terminus, which also includes Asp38, has been shown to be involved in the binding of CYP101 (Davies & Sligar, 1992; Roitberg *et al.*, 1998). In the Roitberg study, detailed modeling of the CYP101 complex was based on the locations of Asp34, Asp38 and Trp106 in the NMR structure of Pdx. In general, the crystal structures of Pdx are significantly different from the NMR structures. To some extent this is likely to reflect the different methods: the molecule in solution is more mobile and many surface residues, *e.g.* Trp106, are probably somewhat conformationally heterogeneous. However, since several key residues have been found in new locations, it may be worthwhile revisiting the modeling of these complexes and the associated electron-transfer mechanisms.

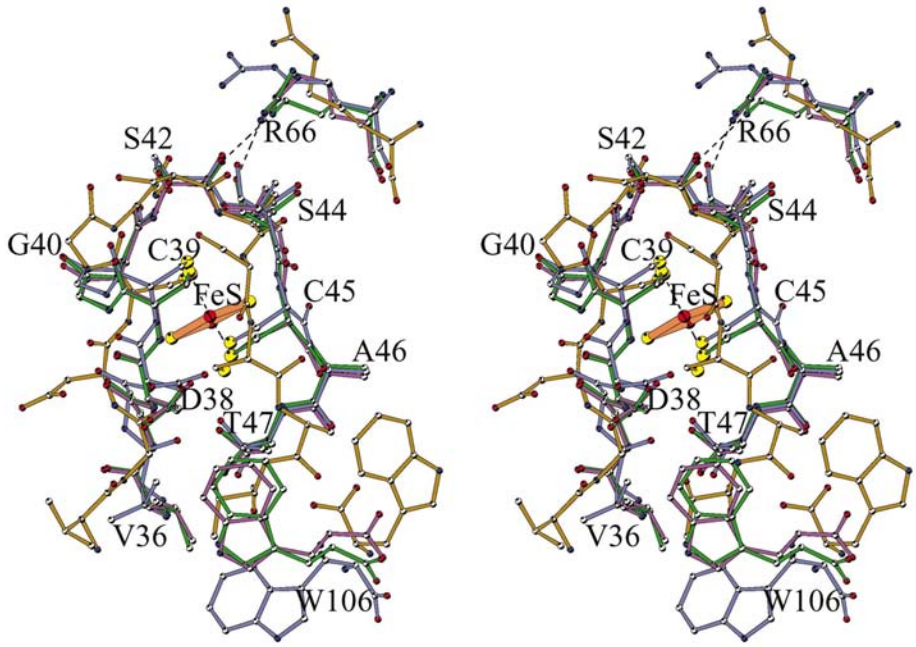

Figure 5
Comparison of four key Pdx structures in the Fe region. Superimposed are 1r7s molecule *A* (green; this work), 1pdx model 1 (brown, NMR; Pochapsky *et al.*, 1994), 1oqq molecule *A* (blue, Sevrioukova *et al.*, 2003) and 1oqr molecule *B* (violet; Sevrioukova *et al.*, 2003). For simplicity, only one of the Fe_2S_2 clusters is shown (orange bonds in center). Dashed lines show the two Cys–Fe1 coordination bonds (from Cys39 and Cys45) and the two 2.9 Å hydrogen bonds from Arg66 to the cluster loop in 1r7s molecule *A* (Arg66 NE–Ser42 O and Arg66 NH2–Ser44 OG). The 1oqr (violet) structure aligns most closely with the green structure, but differs in the rotamer of Ser44, thus lacking this hydrogen bond to Arg66. The 1r7s and 1oqr structures have Ala46 in an Lα conformation, while the others do not. For Trp106, all but one of the X-ray structures have the same location: the 1oqq molecule *A* structure (blue) has Trp106 in a unique location, while the NMR structures vary. The figure was produced using *MOLSCRIPT* (Kraulis, 1991).

The authors gratefully acknowledge the assistance of Salita Kaistha

and Jaya Moses in crystal screening, cultivation and photography. Data for this study were measured at beamline X26c of the National Synchrotron Light Source; financial support for this beamline comes principally from the National Center for Research Resources of the National Institutes of Health and from the Offices of Biological and Environmental Research and of Basic Energy Sciences of the US Department of Energy. Identification of specific instruments and products in this paper is solely to identify the experimental procedure and does not imply recommendation or endorsement.

References

Berman, H. M., Battistuz, T., Bhat, T., Bluhm, N. W. F., Bourne, P. E., Burkhardt, K., Feng, Z., Gilliland, G. L., Iype, L., Jain, S., Fagan, P., Marvin, J., Padilla, D., Ravichandran, V., Schneider, B., Thanki, N., Weissig, H., Westbrook, J. D. & Zardecki, C. (2002). *Acta Cryst.* D**58**, 899–907.

Brünger, A. T., Adams, P. D., Clore, G. M., DeLano, W. L., Gross, P., Grosse-Kunstleve, R. W., Jiang, J.-S., Kuszewski, J., Nilges, N., Pannu, N. S., Read, R. J., Rice, L. M., Simonson, T. & Warren, G. L. (1998). *Acta Cryst.* D**54**, 905–921.

Davies, M. D. & Sligar, S. G. (1992). *Biochemistry*, **31**, 11383–11389.

Grayson, D. A., Tewari, Y. B., Mayhew, M. P., Vilker, V. L. & Goldberg, R. N. (1996). *Arch. Biochem. Biophys.* **332**, 239–247.

Holden, M., Mayhew, M., Bunk, D., Roitberg, A. & Vilker, V. (1997). *J. Biol. Chem.* **272**, 21720–21725.

Kostic, M., Pochapsky, S. S., Obenauer, J., Mo, H., Pagini, G. M., Pejchal, R. & Pochapsky, T. C. (2002). *Biochemistry*, **41**, 5978–5989.

Kraulis, P. J. (1991). *J. Appl. Cryst.* **24**, 946–950.

Laskowski, R. A., MacArthur, M. W., Moss, D. S. & Thornton, J. M. (1993). *J. Appl. Cryst.* **26**, 283–291.

Lyons, T. A., Ratnaswamy, G. & Pochapsky, T. C. (1996). *Protein Sci.* **5**, 627–639.

McRee, D. (1999). *J. Struct. Biol.* **125**, 156–165.

Morales, R., Chron, M., Hudry-Clergeon, G., Petillot, Y., Norager, S., Medina, M. & Frey, M. (1999). *Biochemistry*, **38**, 15764–15773.

Mueller, E. J., Loida, P. J. & Sligar, S. G. (1995). *Cytochrome P450: Structure, Mechanism and Biochemistry*, 2nd ed., edited by P. R. Ortiz de Montellano, pp. 83–124. New York: Plenum Press.

Muller, J. J., Lapko, A., Bourenkov, G., Ruckpaul, K. & Heinemann, U. (2001). *J. Biol. Chem.* **276**, 2786–2789.

Otwinowski, Z. & Minor, W. (1997). *Methods Enzymol.* **276**, 307–326.

Pochapsky, T. C., Ye, X. M., Ratnaswamy, G. & Lyons, T. A. (1994). *Biochemistry* **33**, 6424–6432.

Richardson, J. & Richardson, D. (1989). *Prediction of Protein Structure and the Principles of Protein Conformation*, edited by G. Fasman & X. Chu, pp. 3–8. New York: Plenum Press.

Roitberg, A. E., Holden, M. J., Mayhew, M. P., Kurnikov, I. V., Beratan, D. N. & Vilker, V. L. (1998). *J. Am. Chem. Soc.* **120**, 8927–8932.

Sari, N., Holden, M. J., Mayhew, M. P., Vilker, V. L. & Coxon, B. (1999). *Biochemistry*, **38**, 9862–9871.

Sevrioukova, I. F., Garcia, C., Li, H., Bhaskar, B. & Poulos, T. L. (2003). *J. Mol. Biol.* **333**, 377–392.

Terwilliger, T. C. & Berendsen, J. (1999). *Acta Cryst.* D**55**, 849–861.

Unno, M., Shimada, H., Toba, Y., Makino, R. & Ishimura, Y. (1996). *J. Biol. Chem.* **271**, 17869–17874.

Vijay-Kumar, S., Bugg, C. E. & Cook, W. J. (1987). *J. Mol. Biol.* **194**, 531–544.

Yeh, A. P., Chatelet, C., Soltis, S. M., Kuhn, P., Meyer, J. & Rees, D. C. (2000). *J. Mol. Biol.* **300**, 587–595.